J. Plasma Phys. (2022), *vol*. 88, 905880508 © The Author(s), 2022.
Published by Cambridge University Press
doi:10.1017/S0022377822000927

Modelling the nonlinear plasma response to externally applied three-dimensional fields with the Stepped Pressure Equilibrium Code

A.M. Wright [1],†, **P. Kim** [2], **N.M. Ferraro** [1] **and S.R. Hudson** [1]

[1]Princeton Plasma Physics Laboratory, Princeton, NJ 08540, USA

[2]Institute for Research in Electronics and Applied Physics, University of Maryland, College Park, MD 20742, USA

(Received 21 January 2022; revised 8 September 2022; accepted 12 September 2022)

Small-amplitude, symmetry-breaking magnetic field perturbations, including resonant magnetic perturbations (RMPs) and error fields, can profoundly impact plasma properties in both tokamaks and stellarators. In this work, we perform the first comparison between the Stepped Pressure Equilibrium Code (SPEC) (a comparatively fast and efficient equilibrium code based on energy-minimisation principles) and M3D-C^1 (a high-fidelity albeit computationally expensive initial-value extended-magnetohydrodynamic (MHD) code) to assess the conditions under which SPEC can be used to model the nonlinear, non-ideal plasma response to an externally applied ($m = 2, n = 1$) RMP field in an experimentally relevant geometry. We find that SPEC is able to capture the plasma response in the weakly nonlinear regime – meaning perturbation amplitudes below the threshold for break up of the separatrix and onset of secondary magnetic island formation – when around half of the total toroidal flux is enclosed in the volume containing the $q = 2$ resonant surface. The observed dependence of SPEC solutions on input parameters, including toroidal flux and the number of volumes into which the plasma is partitioned, indicates that additional exploration of the underlying Multi-Region Relaxed MHD physics model is needed to constrain the choice of parameters. Nonetheless, this work suggests promising applications of SPEC to optimisation and fusion plasma design.

Key words: fusion plasma, plasma confinement, plasma nonlinear phenomena

1. Introduction

Small-amplitude, symmetry-breaking magnetic field perturbations can profoundly impact plasma properties in both tokamaks and stellarators (Callen 2011). Externally applied resonant magnetic perturbations (RMPs) form the basis of mitigation strategies for edge-localised modes in tokamaks and will play an important role in ITER (Evans *et al.* 2004, 2006, 2008; Turnbull *et al.* 2013). Unintended three-dimensional (3-D) magnetic field perturbations, known as error fields, can be introduced in a variety of ways, including through coil construction, alignment and positioning, 3-D structures in the vessel wall and

† Email address for correspondence: awright@pppl.gov

blanket materials (Piron *et al.* 2020). Quasisymmetry in stellarators, for example, can be particularly sensitive to error fields which arise due to finite-build coils (Singh *et al.* 2020), misalignment and other coil imperfections (Zhu *et al.* 2019, 2018; Imbert-Gerard, Paul & Wright 2020).

A variety of equilibrium and time-dependent approaches for modelling plasmas in the presence of externally applied, symmetry-breaking magnetic fields have been explored. These include linear (Liu *et al.* 2000; Ferraro *et al.* 2013; Wingen *et al.* 2015) or perturbative methods (Nührenberg & Boozer 2003; Boozer & Nührenberg 2006; Park, Boozer & Glasser 2007; Park & Logan 2017), as well as nonlinear approaches (Izzo & Joseph 2008; Hudson *et al.* 2012; Orain *et al.* 2014; Suzuki 2017). For detailed discussions see Turnbull (2012); Turnbull *et al.* (2013) and Reiman *et al.* (2015) and references therein.

It has been argued (Turnbull 2012) that linear and perturbative methods are insufficient to completely model the effect of symmetry-breaking magnetic field perturbations, which induces both an ideal and a non-ideal response in the plasma. Even in a linear ideal magnetohydrodynamic (MHD) model, these perturbations can change the shape of the plasma and, consequently, can qualitatively modify MHD stability boundaries (Hegna 2014). Perturbative methods, particularly those which seek to identify nearby 'perturbed equilibria', do not explicitly account for dynamical accessibility so there is no guarantee that these states will (or even can) be reached by a dynamically evolving plasma (Turnbull 2012).

Presently, there exist few numerical tools capable of modelling – at least, in principle – both nonlinear and non-ideal effects due to externally applied, symmetry-breaking magnetic field perturbations in realistic toroidal geometries. Among these are extended-MHD codes such as M3D-C^1 (Jardin *et al.* 2012), NIMROD (Sovinec *et al.* 2003) and JOREK (Hoelzl *et al.* 2021), and MHD equilibrium codes such as the Stepped Pressure Equilibrium Code (SPEC) (Hudson *et al.* 2012), HINT2 (Suzuki *et al.* 2006), PIES (Reiman & Greenside 1986) and SIESTA (Hirshman, Sanchez & Cook 2011), which do not assume continuously nested flux surfaces. Unlike extended-MHD codes, most MHD equilibrium codes do not explicitly calculate the time-dependent dynamics associated with the evolution of the plasma (a notable exception being HINT2 which obtains equilibria as the long-time solution of a reduced time-evolution model Park *et al.* 1986). Instead, a time-independent state, consistent with the physics assumptions of each code's underlying reduced model, is returned. In contrast to extended-MHD codes, this means that most equilibrium codes are not guaranteed to produce a solution that closely approximates the actual plasma evolution, i.e. a dynamically accessible state. However, when they do, non-ideal equilibrium codes can be particularly useful since they are much faster and less computationally expensive than extended-MHD codes.

In this work we are interested in examining the conditions under which SPEC (Hudson *et al.* 2012) recovers the same nonlinear, non-ideal plasma response to externally applied symmetry-breaking magnetic field perturbations as an extended-MHD model. This is determined by comparing SPEC solutions with nonlinear simulations with the extended-MHD code, M3D-C^1. SPEC is based on the Multi-Region Relaxed MHD (MRxMHD) physics model (Hole, Hudson & Dewar 2007) and involves partitioning the plasma into a finite number of volumes (denoted by N_{vol}) across which the pressure is constant so that the magnetic field is force free in each volume. Importantly, while SPEC has several modes of operation, only one of these is based on the MRxMHD model; namely, where the magnetic helicity in each volume is held fixed during the solution procedure. In Cartesian slab geometry it has been shown that, when N_{vol} is very large, SPEC produces magnetic islands that are consistent with saturated tearing mode islands obtained from solving a time-dependent resistive MHD model (Loizu *et al.* 2020). Also,

https://doi.org/10.1017/S0022377822000927 Published online by Cambridge University Press

in Cartesian slab geometry, it was recently shown (Huang *et al.* 2021) that SPEC can recover the expected response of the Hahm–Kulsrud forced reconnection problem (Hahm & Kulsrud 1985) in the limit $N_{\mathrm{vol}} \gg 1$.

For actual and experimentally relevant use cases, however, SPEC calculations are performed with only a small number of volumes. For example, a recent application of SPEC to model current crashes in the Wendelstein 7-X stellarator used five volumes (Aleynikova *et al.* 2021). In part, this is due to present limitations in code performance (with respect to both speed and convergence) in realistic geometries. More generally, however, since the ideal MHD model is well established and there exist robust and efficient ideal MHD equilibrium solvers, e.g. VMEC (Hirshman & Whitson 1983), the utility of MRxMHD is not in the $N_{\mathrm{vol}} \gg 1$ limit, but rather when N_{vol} is relatively small. The veracity of the underlying physics model in this regime remains largely untested and, therefore, motivates this work.

An important consideration when applying the MRxMHD model is deciding how to choose N_{vol}. In the MRxMHD model, KAM theory (Kolmogorov 1954; Möser 1962; Arnold 1963) is invoked to justify the existence of the interfaces that separate adjacent plasma volumes, in the absence of axisymmetry. This, in turn, constrains but does not necessarily specify N_{vol}, leaving some freedom to choose N_{vol}, particularly in the small volume and/or weakly non-axisymmetric limit. As far as we are aware, there is currently no standardised approach to selecting N_{vol} in these cases. In § 3 we discuss in greater detail some considerations that affect the choice of N_{vol} for this work. We find that the normalised toroidal flux in the volume containing the resonant surface of interest determines the key physics properties of interest in the SPEC solution (e.g. magnetic island width). Thus, for the purposes of the present study we focus on the dependence of solutions on toroidal flux which, together with N_{vol}, is one of several input parameters that need to be specified. As a consequence, for tractability we consider a single choice of $N_{\mathrm{vol}} = 5$ since it is the same as that which was recently used by Aleynikova *et al.* (2021).

Our paper is subsequently organised as follows. In § 2 we present the equilibrium profiles used for this study and characterise the linear stability properties. In § 3 we discuss discretisation of the equilibrium profiles and the SPEC workflow for experimentally relevant use cases. In § 4 we describe how externally applied symmetry-breaking magnetic field perturbations are represented in SPEC and M3D-C^1. In § 5 we present parameter scans and compare SPEC solutions with M3D-C^1 simulations of the nonlinear, non-ideal plasma response to $(m = 2, n = 1)$ RMP fields. Finally, discussion and conclusions are presented in § 6.

2. Characterisation of equilibrium properties

In this work we consider a circular cross-section tokamak that is modelled by a periodic cylinder with radius $a = 1$ m and axial period $2\pi R_0$ where $R_0 = 10$ m is the analogue of the major radius in toroidal geometry. This approximation is valid in the large aspect ratio limit and has the advantage of eliminating poloidal mode coupling. As will be seen in § 4, the latter allows us to prescribe an RMP field with a single poloidal and toroidal mode number (m and n, respectively) in the M3D-C^1 model. The equilibrium safety factor and pressure profiles are given by

$$q = q_0 \left[1 + x^2 \left(\frac{q_a}{q_0} - 1 \right) \right], \tag{2.1}$$

$$p = p_0 \left(1 - x^2 \right)^2, \tag{2.2}$$

https://doi.org/10.1017/S0022377822000927 Published online by Cambridge University Press

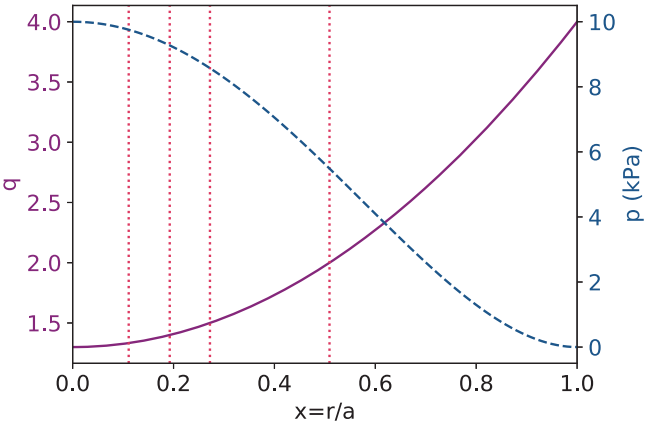

FIGURE 1. Equilibrium safety factor (q, solid) and pressure (p, dashed) profiles. Here, $q_0 = 1.3$, $q_a = 4$ and $\beta = 0.82\,\%$. Mode rational surfaces, located at $x_s = \{0.11, 0.19, 0.27, 0.51\}$ and corresponding to $q(x_s) = \{4/3, 7/5, 3/2, 2\}$, respectively, are indicated by vertical dotted lines.

respectively, where $x = r/a$ is a normalised radial coordinate, $q_0 = 1.3$ and $p_0 = 10^4$ Pa are the values of q and p at the magnetic axis and $q_a = 4$ is the value of q at the plasma edge. This corresponds to a volume-averaged plasma β of 0.82 %. The equilibrium q and p profiles are shown in figure 1.

2.1. *Tearing and interchange stability*

To determine stability with respect to ideal interchange modes, we evaluate Suydam's criterion (Hosking & Dewar 2016) at several resonant surfaces of interest. Recall that

$$xB_z^2(x)\left[\frac{q'(x)}{q(x)}\right]^2 + 8\mu_0 p'(x) > 0, \tag{2.3}$$

is required for stability, where $'$ denotes differentiation with respect to x, B_z is the axial component of the equilibrium magnetic field and μ_0 is the vacuum permeability. Specifically, we consider the $(m = 2, n = 1)$, $(m = 3, n = 2)$, $(m = 4, n = 3)$, $(m = 6, n = 4)$ and $(m = 7, n = 5)$ modes which are associated with the following set of low-order mode rational surfaces; $q(x_s) = \{2, 1.5, 1.33, 1.4\}$ where $x_s = \{0.51, 0.27, 0.11, 0.19\}$, respectively. The mode rational surfaces are shown in figure 1. Of these, only the $(m = 4, n = 3)$ mode is interchange unstable.

Next, linear stability with respect to tearing modes is determined by evaluating the usual Δ' parameter at the resonant surfaces of interest, x_s, which are such that $q(x_s) = m/n$ for a particular (m, n) mode. Recall that (Furth, Rutherford & Selberg 1973),

$$\Delta' \equiv \frac{\lim\limits_{x\to x_s^+}\psi'(x) - \lim\limits_{x\to x_s^-}\psi'(x)}{a\psi(x_s)} < 0, \tag{2.4}$$

is required for stability, where $\psi(x)$ is a solution of the Euler–Lagrange equation that follows from the Energy Principle (e.g. see (1) from Furth *et al.* 1973). The requisite boundary conditions are $\psi(0) = 0$ if $m \neq \pm 1$, $\psi'(0) = 0$ if $m = \pm 1$ and $\psi(1) = 0$ with $\psi(x_s) = \psi_0$ for some $\psi_0 = \text{const.} > 0$. Applied to the modes of interest, we find that the

https://doi.org/10.1017/S0022377822000927 Published online by Cambridge University Press

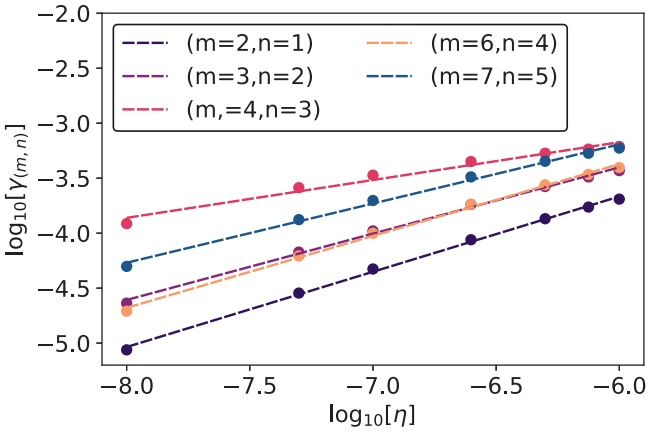

FIGURE 2. Non-ideal linear growth rates, $\gamma_{(m,n)}$, computed using M3D-C^1 for toroidal mode numbers $1 \leq n \leq 5$. In each case, the poloidal mode number, m, corresponds to that of the fastest growing linear instability. The dependence of $\gamma_{(m,n)}$ on resistivity, η, indicates these are resistive modes. In particular, $\gamma_{(2,1)} \sim \eta^{0.684}$, $\gamma_{(3,2)} \sim \eta^{0.603}$, $\gamma_{(4,3)} \sim \eta^{0.344}$, $\gamma_{(6,4)} \sim \eta^{0.653}$ and $\gamma_{(7,5)} \sim \eta^{0.538}$.

$(m = 2, n = 1)$, $(m = 3, n = 2)$, $(m = 6, n = 4)$ and $(m = 7, n = 5)$ modes are tearing unstable since $\Delta' > 0$ in all cases.

2.2. *Non-ideal linear growth rates*

To compute linear growth rates and verify the characterisation given in § 2.1, we use the linear version of M3D-C^1. Specifically, we calculate the non-ideal (linear) growth rates, $\gamma_{(m,n)}$, for $1 \leq n \leq 5$. For each n, the corresponding m is that associated with the fastest growing linear instability. We perform a series of parameter scans with varying resistivity, η, to determine the scaling of $\gamma_{(m,n)}$ with respect to resistivity, which allows us to classify the dominant linear instabilities.

The growth rates for modes with $1 \leq n \leq 5$ are shown in figure 2 and calculated for $\eta \in [10^{-8}, 10^{-6}]$ and $\nu = 10^{-7}$, where ν is the viscosity. The parameter range considered is equivalent to $\eta \in [0.0274, 2.741]$ Ωm in SI units, $S \in [7.96 \times 10^5, 7.96 \times 10^7]$ and $P_m \in [0.1, 10]$, where the Lundquist number, S, is the ratio of the resistive and Alfvénic time scales and $P_m \equiv \nu/\eta$ is the magnetic Prandtl number. For each n considered, the poloidal mode number of the most unstable mode coincides with those considered in § 2.1. This is as expected since the $(m = 2, n = 1)$, $(m = 3, n = 2)$, $(m = 4, n = 3)$, $(m = 6, n = 4)$ and $(m = 7, n = 5)$ modes are associated with mode rational surfaces of relatively low order. We observe that the growth rate for each of these modes scales linearly on a log–log plot, indicating that they are all of resistive character. In particular, we find $\gamma_{(2,1)} \sim \eta^{0.684}$, $\gamma_{(3,2)} \sim \eta^{0.603}$, $\gamma_{(4,3)} \sim \eta^{0.344}$, $\gamma_{(6,4)} \sim \eta^{0.653}$ and $\gamma_{(7,5)} \sim \eta^{0.538}$. Of these, $\gamma_{(2,1)}$, $\gamma_{(3,2)}$ and $\gamma_{(6,4)}$ agree well with the theoretical scaling for tearing modes (Wesson & Campbell 2011), which goes like $\gamma \propto \eta^{3/5}$. Similarly, $\gamma_{(7,5)}$ agrees qualitatively. This is consistent with the classification of these instabilities as tearing modes. By contrast, the dependency of $\gamma_{(4,3)}$ on η is much weaker.

In § 5, we will consider and compare the nonlinear plasma responses to externally applied $(m = 2, n = 1)$ RMP fields as calculated by M3D-C^1 and SPEC, for the equilibrium specified by (2.1) and (2.2). Whereas the preceding analysis shows that this equilibrium is linearly unstable, figure 3 also indicates that $\gamma_{(m,n)}$ depends strongly on

https://doi.org/10.1017/S0022377822000927 Published online by Cambridge University Press

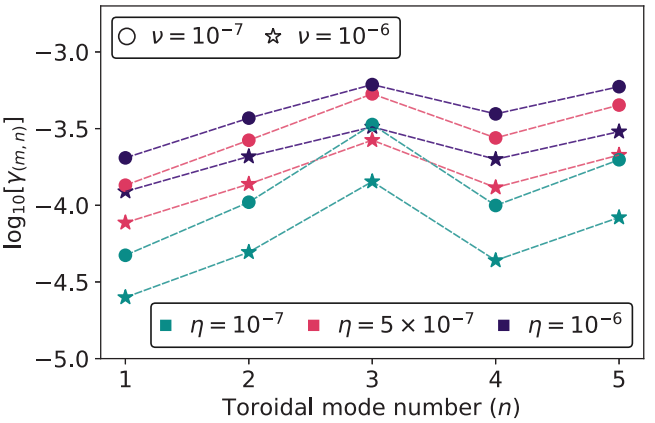

FIGURE 3. Non-ideal linear growth rates, $\gamma_{(m,n)}$, computed using M3D-C^1 for $\nu = 10^{-7}$ (circles) and $\nu = 10^{-6}$ (stars) and three different values of resistivity, η.

the viscosity, ν. This is as expected and, based on figure 3, we find that increasing the viscosity by an order of magnitude reduces the growth rate by approximately half an order of magnitude. For the nonlinear studies, we use $P_m = 1$. We will find that growth of the $(m = 4, n = 3)$ interchange mode is largely damped out in the nonlinear M3D-C^1 simulations. In addition, the resistive instabilities are sufficiently slow growing that there is adequate separation between growth of these modes and saturation of the $(m = 2, n = 1)$ magnetic island associated with the applied RMP.

3. Profile discretisation and SPEC workflow

With the (smooth) equilibrium profiles characterised, we now consider the discretisation of these profiles and preparation of input profiles for SPEC. In MRxMHD (Hudson *et al.* 2012), the plasma is partitioned into N_{vol} concentrically nested volumes. Each volume is separated by an interface across which a discontinuity in the pressure can be supported. Within each ith volume, the pressure (p_i) is constant. Thus, the magnetic field in each volume $(\boldsymbol{B}_i)$ is assumed to be force free, satisfying

$$\nabla \times \boldsymbol{B}_i = \mu_i \boldsymbol{B}_i. \tag{3.1}$$

Here, μ_i is a constant and can be related to the parallel current density by taking the dot product of (3.1) with $\boldsymbol{B}_i$. In general, p_i and μ_i will differ between volumes. Each interface is required to satisfy a jump condition (Hole *et al.* 2007),

$$\left[\left[\frac{B_i^2}{2\mu_0} + p_i\right]\right] = 0, \tag{3.2}$$

which ensures that the total pressure (magnetic plus thermal) is continuous. Depending on the mode of operation, specific combinations of input parameters are held fixed while the geometry of the interfaces is varied at each iteration to satisfy (3.2).

As alluded to in § 1, SPEC currently has at least three modes of operation. In all cases, the pressure is approximated by a piecewise constant profile and held fixed. In each volume, the toroidal flux $(\Psi_{t,i})$, poloidal flux $(\Psi_{p,i})$, volume-averaged magnetic helicity $(\mathcal{K}_i)$ and μ_i also need to be specified. Depending on the mode of operation, particular combinations of these parameters are held fixed. Details of the calculation of these

https://doi.org/10.1017/S0022377822000927 Published online by Cambridge University Press

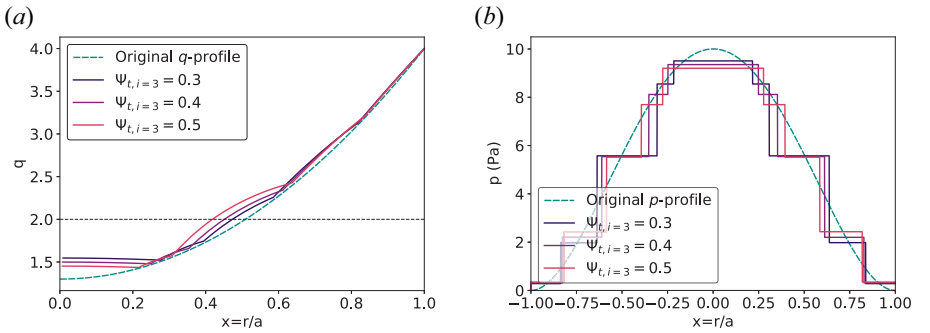

FIGURE 4. The original (green, dashed) and discretised (*a*) q-profiles and (*b*) pressure profiles for $\Psi_{t,i=3} = 0.3$ (blue), 0.4 (purple) and 0.5 (pink), where $\Psi_{t,i=3}$ is the normalised toroidal flux in the volume containing the $q = 2$ resonance (*a*, horizontal dashed line). The original profiles are given by (2.1) and (2.2), respectively. The discretised profiles are obtained from SPEC by running in 'fixed iota' mode and enforcing axisymmetry. See figure 5 for a summary of the procedure.

quantities in cylindrical geometry may be found in Hole, Hudson & Dewar (2006). In addition, the value of the rotational transform, $\iota \equiv 1/q$, on either side of each interface may be required.

In the so-called 'fixed helicity' mode, the toroidal flux and helicity in each volume are held fixed. This mode is the one that corresponds to the assumptions of the MRxMHD model and, therefore, in this work we consider only solutions that are calculated using the fixed helicity method (Hudson *et al.* 2012).

Although an essential feature of the MRxMHD model, the number of volumes N_{vol} is usually a free parameter in practice. In the MRxMHD model, the interfaces are associated with invariant KAM surfaces (Hole *et al.* 2006). Therefore, in the absence of axisymmetry, the rotational transform on each interface is required to satisfy specific properties (McGann *et al.* 2010), that effectively depend on the strength of the non-axisymmetry. This constrains the values of the rotational transform for which interfaces may be supported and effectively fixes the discretisation of the pressure profile. If, however, the interface geometry is independent of the toroidal-like angle, ϕ, then there exists a continuous symmetry. As a consequence, the preceding restrictions do not apply and we are also free to prescribe the initial positions of the interfaces.

Despite – or, perhaps as a consequence of – the flexibility of SPEC to compute solutions to (3.1) and (3.2) subject to different constraints, there does not currently exist a standardised or self-consistent approach for transforming smooth profiles (e.g. obtained from experimental reconstruction) into the piecewise constant representation required by SPEC. Thus, in this work we propose and describe one approach that is based on the experimentally motivated use cases of SPEC.

We consider a piecewise constant pressure profile obtained by discretising (2.2) using 5 volumes. Specifically, we take the value of the pressure in each volume to be the volume-averaged pressure calculated from (2.2). In this case, we have chosen $N_{\mathrm{vol}} = 5$ to ensure that the original q-profile is well approximated, while still keeping the total number of volumes relatively small. The original and discretised pressure profiles and q-profiles are given in figure 4.

The workflow used to compute SPEC solutions with fixed helicity is summarised in figure 5. Our aim is to consider experimentally relevant use cases, so our procedure starts

https://doi.org/10.1017/S0022377822000927 Published online by Cambridge University Press

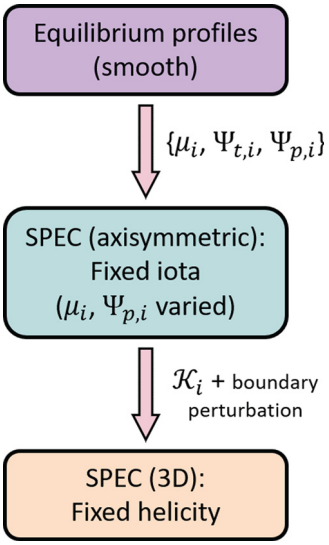

FIGURE 5. Summary of the workflow used to calculate a nonlinear, non-ideal response to externally applied, symmetry-breaking magnetic field perturbations using SPEC. The equilibrium profiles are used to calculate the toroidal and poloidal fluxes in each volume, $\Psi_{t,i}$ and $\Psi_{p,i}$. The parallel current density is discretised to obtain μ_i. SPEC's 'fixed iota' mode is then used to obtain the volume-averaged helicity, $\mathcal{K}_i$, in each volume. In this first calculation, axisymmetry is enforced by setting the toroidal Fourier resolution parameter equal to zero. The SPEC boundary is then deformed to model the effect of an externally applied magnetic field perturbation. Finally, with $\mathcal{K}_i$, μ_i, $\Psi_{t,i}$ and $\Psi_{p,i}$ as inputs in each volume, SPEC's fixed helicity mode is used to calculate a nonlinear, non-ideal response to the applied magnetic field perturbation.

with smooth initial profiles for q and p. In this work, q and p are given by (2.1) and (2.2). However, these could readily be substituted for profiles obtained from experimental reconstruction, e.g. EFIT (Lao *et al.* 1985). From the smooth profiles, we compute the toroidal and poloidal fluxes in each volume, $\Psi_{t,i}$ and $\Psi_{p,i}$. The parallel current density, $J_\parallel$, is discretised using the same approach as is taken for p, to determine μ_i in each volume.

The final radial position of each interface is determined by the toroidal flux enclosed in each volume. As an initial guess, we choose $\Psi_{t,i}$ so that half of the toroidal flux in the volume containing the $q = 2$ rational surface (which is the mode rational surface of interest in this work) is enclosed by that surface. We then distribute $\Psi_{t,i}$ equally in the remaining volumes.

Next, we run SPEC in 'fixed iota' mode, where ι on either side of each interface is held fixed while μ_i and $\Psi_{p,i}$ are varied. As an output, we obtain values for $\mathcal{K}_i$, the volume-averaged helicity in each volume. To preserve a continuous rotational transform profile, ι on either side of each interface is equal and taken from the corresponding value of $q(x_i)$ where x_i is the radial position of each jump in the discretised pressure profile. In this first calculation, axisymmetry is enforced by setting the toroidal Fourier resolution parameter, `ntor`, equal to zero.

With values for $\mathcal{K}_i$, μ_i, $\Psi_{t,i}$ and $\Psi_{p,i}$ in hand, an externally applied, symmetry-breaking magnetic field perturbation is modelled in SPEC by deforming the plasma boundary. As SPEC uses a doubly periodic Fourier representation for the poloidal and toroidal angles, this is achieved by modifying the amplitude of the Fourier component of the boundary

https://doi.org/10.1017/S0022377822000927 Published online by Cambridge University Press

representation corresponding to the particular (m, n) mode of the external perturbation. SPEC is then run in fixed helicity mode. Non-axisymmetric solutions are admitted by choosing the poloidal and toroidal Fourier resolution parameters so that `mpol` > 0 and `ntor` > 0, respectively. The resultant solution corresponds to the nonlinear, non-ideal response associated with the prescribed externally applied, symmetry-breaking magnetic field perturbation.

4. The RMP models and coordinate systems

Before proceeding to a comparison of results, in this section we describe the methods and coordinate systems that are used to model externally applied magnetic field perturbations in SPEC and M3D-C^1.

4.1. *Coordinate systems*

For the periodic, cylindrical geometry considered in this work, quantities in SPEC and M3D-C^1 can be described using the same Cartesian coordinate system, with orthonormal basis vectors $\{\hat{\boldsymbol{i}}, \hat{\boldsymbol{j}}, \hat{\boldsymbol{k}}\}$. A position vector, $\boldsymbol{r}$, can be decomposed as

$$\boldsymbol{r}_{\text{SPEC}} = r\cos\theta\hat{\boldsymbol{i}} + r\sin\theta\hat{\boldsymbol{j}} + \zeta\boldsymbol{k}, \tag{4.1}$$

$$\boldsymbol{r}_{\text{M3D-C}^1} = r\cos\theta\hat{\boldsymbol{i}} + r\sin\theta\hat{\boldsymbol{j}} + z/R_0\boldsymbol{k}, \tag{4.2}$$

in SPEC and M3D-C^1, respectively. From (4.1) and (4.2), we can define cylindrical coordinates, $\{r, \theta, \zeta\}$ and $\{r, \theta, z\}$, for SPEC and M3D-C^1, respectively. Since ζ and z are analogues of the toroidal angle, ϕ, both ζ and z/R_0 must be 2π-periodic and such that $\zeta = z/R_0$. To distinguish the latter from the cylindrical coordinates used by M3D-C^1 in a toroidal geometry and which are usually denoted $\{R, \phi, Z\}$, we refer to $\{r, \theta, z\}$ as the 'local' cylindrical coordinates.

4.2. *Boundary representation in SPEC*

For this work, we use the fixed-boundary version of SPEC. In this case, an externally applied magnetic field perturbation is modelled by modifying the shape of the plasma boundary, which is a required input parameter. For a periodic cylinder, the boundary shape is specified by $r_b(\theta, \zeta)\cos\theta\hat{\boldsymbol{i}} + r_b(\theta, \zeta)\sin\theta\hat{\boldsymbol{j}} + \zeta\hat{\boldsymbol{k}}$. The scalar function $r_b(\theta, \zeta)$ is given by the following stellarator symmetric Fourier representation (Hudson *et al.* 2012):

$$r_b(\theta, \zeta) = \sum_i r_i \cos\left(m_i\theta - n_i\zeta\right), \tag{4.3}$$

where $\{r_i\}$ are the Fourier coefficients and i indexes every unique ordered pair $\{m_i, n_i\}$ for $m_i \in [0, \texttt{mpol}]$ and $n_i \in [0, \texttt{ntor}]$. Therefore, for an externally applied (m, n) magnetic field perturbation, the perturbed boundary in SPEC is given by

$$r_{b,\text{RMP}}(\theta, \zeta) = a + \Delta r_a \cos\left(m\theta - n\zeta\right), \tag{4.4}$$

where Δr_a denotes the magnitude of the non-axisymmetric perturbation. Clearly, when $\Delta r_a \to 0$, (4.4) reduces to the circular cross-section configuration with minor radius $a = 1$ m of the axisymmetric equilibrium given in § 2. In this work, we consider only the case where a single (m, n) perturbation field is applied for $0.01\text{ mm} \leq \Delta r_a < 2\text{ mm}$. However, it is straightforward to generalise to an externally applied field with multiple harmonics.

https://doi.org/10.1017/S0022377822000927 Published online by Cambridge University Press

4.3. *Representation of RMP fields in M3D-C*^{1}

In M3D-C^1, several different approaches for modelling RMP and error fields have been implemented and are regularly used to study the plasma response (Ferraro 2012; Ferraro *et al.* 2013; Reiman *et al.* 2015; Wingen *et al.* 2015; Canal *et al.* 2017; Lyons *et al.* 2017). Moreover, the recent extension of M3D-C^1 to stellarator geometry (Zhou *et al.* 2021) affords additional capability to self-consistently model plasma evolution in the presence of strong non-axisymmetric external fields.

For this work, the externally applied magnetic field perturbation is modelled in M3D-C^1 by a vacuum field, $\boldsymbol{B}_{\mathrm{RMP}}$, so that the total magnetic field, $\boldsymbol{B}$, is given by $\boldsymbol{B} = \boldsymbol{B}_{\mathrm{plasma}} + \boldsymbol{B}_{\mathrm{RMP}}$. From this definition, $\boldsymbol{B}_{\mathrm{RMP}}$ satisfies,

$$\boldsymbol{\nabla} \times \boldsymbol{B}_{\mathrm{RMP}} = 0, \tag{4.5}$$

$$\boldsymbol{\nabla} \cdot \boldsymbol{B}_{\mathrm{RMP}} = 0. \tag{4.6}$$

Importantly, in cylindrical geometry, the absence of poloidal mode coupling makes it possible to impose an RMP field associated with a single poloidal and toroidal mode number.

Using the local cylindrical coordinates $\{r, \theta, z\}$ we can expand the differential operators in (4.5) and (4.6) according to their usual definitions. From (4.5) and (4.6) it follows that $\boldsymbol{B}_{\mathrm{RMP}} = \boldsymbol{\nabla} M(r, \theta, z)$, where $M(r, \theta, z)$ is a scalar function satisfying

$$\nabla^2 M(r, \theta, z) = 0. \tag{4.7}$$

Assuming boundedness at $r = 0$ and 2π-periodic boundary conditions in θ and z, the general solution of (4.7) is given by

$$M(r, \theta, z) = \delta B_r \alpha^{-1} I_m\,(nr/R_0)\ \mathrm{e}^{-\mathrm{i}m\theta}\ \mathrm{e}^{\mathrm{i}nz/R_0}, \tag{4.8}$$

where $I_m\,(x)$ is a modified Bessel function of the first kind and α and δB_r are some constants. The exponential terms in (4.8) correspond to a 'phase factor' which we denote by $\Phi(\theta, z)$ for convenience. Thus, in cylindrical $\{r, \theta, z\}$-coordinates, the components of $\boldsymbol{B}_{\mathrm{RMP}}$ are given by

$$B_{r,\mathrm{RMP}}(r, \theta, z) = \frac{\delta B_r n}{2R_0}\left[I_{m-1}\left(\frac{nr}{R_0}\right) + I_{m+1}\left(\frac{nr}{R_0}\right)\right]\frac{\Phi(\theta, z)}{\alpha}, \tag{4.9}$$

$$B_{\theta,\mathrm{RMP}}(r, \theta, z) = -\frac{\mathrm{i}\delta B_r m}{r} I_m\left(\frac{nr}{R_0}\right)\frac{\Phi(\theta, z)}{\alpha}, \tag{4.10}$$

$$B_{z,\mathrm{RMP}}(r, \theta, z) = \mathrm{i}\delta B_r n I_m\left(\frac{nr}{R_0}\right)\frac{\Phi(\theta, z)}{\alpha}, \tag{4.11}$$

where α is chosen so that $B_{r,\mathrm{RMP}}(r = 1, \theta, z) = \delta B_r \Phi(\theta, z)$ yielding

$$\alpha = \frac{n}{2R_0}\left[I_{m-1}\left(\frac{n}{R_0}\right) + I_{m+1}\left(\frac{n}{R_0}\right)\right]. \tag{4.12}$$

4.4. *Relating the M3D-C*^{1} *and SPEC representations of RMP fields*

Whereas an externally applied magnetic field perturbation in SPEC is modelled by specifying the amplitude of a deformation of the plasma boundary, Δr_a, in M3D-C^1 the

https://doi.org/10.1017/S0022377822000927 Published online by Cambridge University Press

amplitude of the field at the plasma boundary, δB_r, is prescribed. In order to compare the M3D-C^1 and SPEC parameters, we now derive a relationship between Δr_a and δB_r.

Recall that the total magnetic field in M3D-C^1 is given by $\boldsymbol{B} = \boldsymbol{B}_{\text{plasma}} + \boldsymbol{B}_{\text{RMP}}$, i.e. the sum of the (nonlinear) plasma response and the vacuum RMP field. In this work, we consider small-amplitude external magnetic field perturbations, corresponding to a $\sim 1\,\%$ perturbation of the magnetic field at the plasma edge. Since $\delta B_r \ll 1$, it suffices to use linear theory to relate δB_r to Δr_a.

Let $\boldsymbol{r}(r,\theta,\zeta) = \boldsymbol{r}_0(r,\theta,\zeta) + \boldsymbol{\xi}(r,\theta,\zeta)$ denote a position vector in SPEC, where $\boldsymbol{\xi}(r,\theta,\zeta)$ is a displacement vector that vanishes when $\Delta r_a = 0$. In the $\{\hat{\boldsymbol{r}}, \hat{\boldsymbol{\theta}}, \hat{\boldsymbol{\zeta}}\}$ basis and using (4.4), we can write

$$\boldsymbol{r}_0(r,\theta,\zeta) = a\hat{\boldsymbol{r}} + \theta\hat{\boldsymbol{\theta}} + \zeta\hat{\boldsymbol{\zeta}}, \tag{4.13}$$

$$\boldsymbol{\xi}(r,\theta,\zeta) = \Delta r_a \cos(m\theta - n\zeta)\,\hat{\boldsymbol{r}}. \tag{4.14}$$

Under a linear approximation, the plasma response in M3D-C^1 is given by $\boldsymbol{B} = \boldsymbol{B}_0 + \boldsymbol{B}_{\text{RMP}}$, where $\boldsymbol{B}_0$ is the equilibrium magnetic field described in § 2. Consequently, we can relate $\boldsymbol{B}_{\text{RMP}}$ to $\boldsymbol{\xi}$ using,

$$\boldsymbol{B}_{\text{RMP}} = \boldsymbol{\nabla} \times (\boldsymbol{\xi} \times \boldsymbol{B}_0), \tag{4.15}$$

which follows from the linearised ideal MHD equations.

Using the fact that $\boldsymbol{B}_0(r) = B_{\theta,0}(r)\hat{\boldsymbol{\theta}} + B_{z,0}(r)\hat{\boldsymbol{z}}$, we expand (4.15) in the $\{\hat{\boldsymbol{r}}, \hat{\boldsymbol{\theta}}, \hat{\boldsymbol{\zeta}}\}$ basis assuming that $\boldsymbol{\xi}(r,\theta,z)$ is given by (4.14) with $\zeta = z/R_0$. The radial component, $\hat{\boldsymbol{r}}$, yields

$$\frac{B_{\theta,0}(r)}{r}\frac{\partial \xi_r(r,\theta,z)}{\partial\theta} + B_{z,0}(r)\frac{\partial \xi_r(r,\theta,z)}{\partial z} = B_{r,\text{RMP}}(r,\theta,z). \tag{4.16}$$

Using (4.14) and (4.9) we find,

$$\Delta r_a \left[\frac{mB_{\theta,0}(r)}{r} - \frac{nB_{z,0}(r)}{R_0}\right] \sin(m\theta - nz/R_0) = \text{Im}[B_{r,\text{RMP}}(r,\theta,z)]. \tag{4.17}$$

Evaluating at the boundary, $r = a$, yields

$$\Delta r_a \left[\frac{mB_{\theta,0}(r=a)}{a} - \frac{nB_{z,0}(r=a)}{R_0}\right] = -\frac{\delta B_r n}{2R_0\alpha}\left[I_{m-1}\left(\frac{na}{R_0}\right) + I_{m+1}\left(\frac{na}{R_0}\right)\right]. \tag{4.18}$$

Using the fact that $q = rB_{z,0}/R_0B_{\theta,0}$, it follows that

$$\delta B_r = 2\Delta r_a \frac{\alpha R_0 B_{\theta,0}(r=a)}{a}\left(q_a - \frac{m}{n}\right)\left[I_{m-1}\left(\frac{na}{R_0}\right) + I_{m+1}\left(\frac{na}{R_0}\right)\right]^{-1}, \tag{4.19}$$

where q_a is the edge safety factor. By assumption, we require that $m/n < q_a$ so the right-hand side of (4.19) is always positive.

When $a = 1$, as is the case considered throughout this work, (4.19) reduces to

$$\delta B_r = \Delta r_a n B_{\theta,0}(r=1)\left(q_a - \frac{m}{n}\right), \tag{4.20}$$

or equivalently

$$\delta B_r = \Delta r_a \frac{mB_{z,0}(r=1)}{R_0}\left(\frac{n}{m} - \frac{1}{q_a}\right). \tag{4.21}$$

https://doi.org/10.1017/S0022377822000927 Published online by Cambridge University Press

5. Comparing nonlinear responses to (2, 1) RMP fields

For this study, we focus on the plasma response to an externally applied perturbation with a single helicity, namely $(m = 2, n = 1)$. In the nonlinear calculations that follow, all modes are included in the plasma response (up to the limit of numerical resolution). In SPEC, we consider poloidal and toroidal Fourier resolution up to `mpol` $= 12$ and `ntor` $= 6$, respectively, which we find sufficient to resolve islands that may arise due to resonances other than $q = 2$. And, as M3D-C^1 does not use a spectral representation in the nonlinear calculations, all modes are included in the calculation of the plasma response. In this study, we used 24 toroidal planes for the nonlinear M3D-C^1 simulations.

Since we use the fixed helicity option of SPEC (see figure 5), in this study, the physics of the nonlinear plasma response calculated by SPEC is governed by the (static) MRxMHD model. Therefore, solutions correspond to plasma states that minimise the energy, subject to conservation of the volume-averaged helicity in each volume, i.e. volume-localised Taylor relaxation (Hole *et al.* 2006; Dewar *et al.* 2015).

The second key assumption of the MRxMHD model is the existence and persistence of the ideal current sheet interfaces, that partition the plasma into volumes. One consequence of MRxMHD interfaces is that plasma in different volumes are prevented from mixing since $\boldsymbol{B} \cdot \hat{\boldsymbol{n}} = 0$ is enforced on each interface, where $\hat{\boldsymbol{n}}$ is the unit normal vector. Consequently, the MRxMHD interfaces frustrate radial transport of plasma. Thus, good agreement between the SPEC and M3D-C^1 solutions implies that the RMP does not lead to large-scale transport of plasma, e.g. from the core to the plasma edge. Finally, another consequence of the MRxMHD model is that SPEC solutions do not include flows, in either the initial profiles or nonlinear solution. Therefore, good agreement between SPEC and M3D-C^1 implies that flows do not have a significant impact on the nonlinear plasma RMP response.

In subsequent sections (§§ 5.1–5.3) we will find that the nonlinear plasma response is primarily dominated by formation of an $(m = 2, n = 1)$ island that is associated with the helicity of the applied RMP. As we will see, for low values of the RMP amplitude ($\delta B_r \leq 0.5$ mT) there are conditions under which SPEC and M3D-C^1 show close agreement for the nonlinear plasma response. When this is the case, MRxMHD theory implies that it is the 3-D state associated with saturation of the $(m = 2, n = 1)$ mode that is energetically favourable, i.e. which minimises the energy, even though there may be other modes present (e.g. as suggested by the linear stability analysis of the smooth equilibrium cf. § 2).

Note that if an RMP field with a different helicity were applied, e.g. $(m = 3, n = 2)$ which is resonant at $x_s = 0.27$, one would expect a different 3-D state to be the energy-minimising state. Finally, in tokamak or stellarator geometry where there is poloidal and toroidal Fourier mode coupling, it is plausible that modes associated with other resonant surfaces may contribute more significantly to the minimum energy 3-D solution because of mode coupling effects.

5.1. *Nonlinear RMP response in M3D-C^1*

Starting from the initial axisymmetric equilibrium given by (2.1) and (2.2), we use M3D-C^1 to simulate the full, nonlinear plasma evolution in response to an $(m = 2, n = 1)$ RMP field, which is applied from $t = 0$ and specified by (4.9)–(4.11). Note that, while we consider static equilibria as an initial condition, M3D-C^1 allows for flows to develop self-consistently in the course of the plasma evolution. In all cases, we choose isotropic values of resistivity and viscosity with $\eta = 2.741\ \Omega$m such that $P_m \equiv \nu/\eta = 1$ and $S = 7.96 \times 10^6$, where P_m and S are the magnetic Prandtl number and Lundquist number,

https://doi.org/10.1017/S0022377822000927 Published online by Cambridge University Press

respectively. We use a model for the heat flux density, $\boldsymbol{q}$, that is given by

$$\boldsymbol{q} = -\kappa_t \nabla T - \kappa_\parallel \frac{\boldsymbol{B}\boldsymbol{B} \cdot \nabla T}{B^2}, \tag{5.1}$$

where $\kappa_\parallel/\kappa_t = 10^6$ is the ratio of the parallel to perpendicular heat conductivity coefficients, T is the temperature and no heat source is applied.

In §§ 2.1 and 2.2 we saw that the equilibrium is linearly unstable, including to an $(m = 2, n = 1)$ tearing mode and $(m = 4, n = 3)$ interchange mode. To determine the potential impact of the unstable modes on the nonlinear plasma response, we first performed a preliminary nonlinear study using M3D-C^1 without an RMP field applied. We find that the unstable resistive modes are slow growing, which ensures sufficient separation between growth and saturation of the $(m = 2, n = 1)$ magnetic island that is driven by the RMP, and other instabilities of the equilibrium. In particular, the $(m = 2, n = 1)$ tearing mode is very slow growing, which is consistent with the linear studies described in § 2.2. As indicated in § 2.2, the linear growth rates depend strongly on ν and, for the dissipation and transport parameters used in the nonlinear studies (which represent realistic experimental values), we find that the $(m = 4, n = 3)$ interchange mode is largely damped out. Therefore, for the parameters considered in this study, the plasma evolution in the presence of the RMP is primarily due to the nonlinear plasma response to the externally applied field.

We consider RMP amplitudes in the range $0.1\ \text{mT} \leq \delta B_r \leq 2\ \text{mT}$ and examine the plasma properties at $t = 5000\tau_A$, which we found was sufficient for the plasma response to reach a quasi-steady state. This was determined by examining the growth rate of the kinetic energy. Poincaré sections taken at $t = 5000\tau_A$ for each δB_r considered are shown in figure 6 as a function of poloidal angle and normalised poloidal flux. As expected, when the amplitude of the applied RMP is small ($0.1\ \text{mT} \leq \delta B_r \leq 0.5\ \text{mT}$), we observe saturation of an $(m = 2, n = 1)$ magnetic island at the $q = 2$ surface, that is driven by the externally applied magnetic field.

For intermediate values, where $0.6\ \text{mT} \leq \delta B_r \leq 0.9\ \text{mT}$, we see the formation of secondary island chains about the O-points of the primary $(m = 2, n = 1)$ magnetic island chain. For example, for $\delta B_r = 0.7$ mT, we see a secondary $m = 9$ island chain. As the perturbation amplitude increases and the secondary islands grow larger, nonlinear interactions begin to drive significant chaos, leading to break up of the separatrix associated with the primary $(m = 2, n = 1)$ island. For sufficiently large perturbation amplitudes ($\delta B_r \geq 1$ mT), the primary $(m = 2, n = 1)$ island becomes embedded in, and eventually consumed by, a sea of chaos. In figure 7, we show a selection of Poincaré sections in $r - z$ coordinates which illustrate the different qualitative features associated with the nonlinear plasma response for varying δB_r. Namely, (i) a saturated $(m = 2, n = 1)$ magnetic island ($\delta B_r = 0.1$ mT), (ii) formation of secondary island chains ($\delta B_r = 0.7$ mT), (iii) break up of the separatrix associated with the primary $(m = 2, n = 1)$ island ($\delta B_r = 1$ mT) and, finally, (iv) near-complete stochasticisation of the plasma core ($\delta B_r = 1.5$ mT).

The corresponding pressure profiles taken at a cut along $z = 0$ when $t = 5000\tau_A$ are shown in figure 8. Overlaid for comparison are the discretised pressure profiles used in the SPEC calculations, with $\Psi_{t,i=3} = 0.3$, 0.4 and 0.5. As expected, for $0.1\text{mT} \leq \delta B_r \leq 1.5$ mT we find significant flattening of the pressure profile in regions coinciding with the $(m = 2, n = 1)$ magnetic island. Nonetheless, in all these cases we observe the presence of pressure gradients in regions coinciding with the $(m = 2, n = 1)$ island and magnetic field line chaos. This is attributable to the fact that the M3D-C^1 model accommodates finite

https://doi.org/10.1017/S0022377822000927 Published online by Cambridge University Press

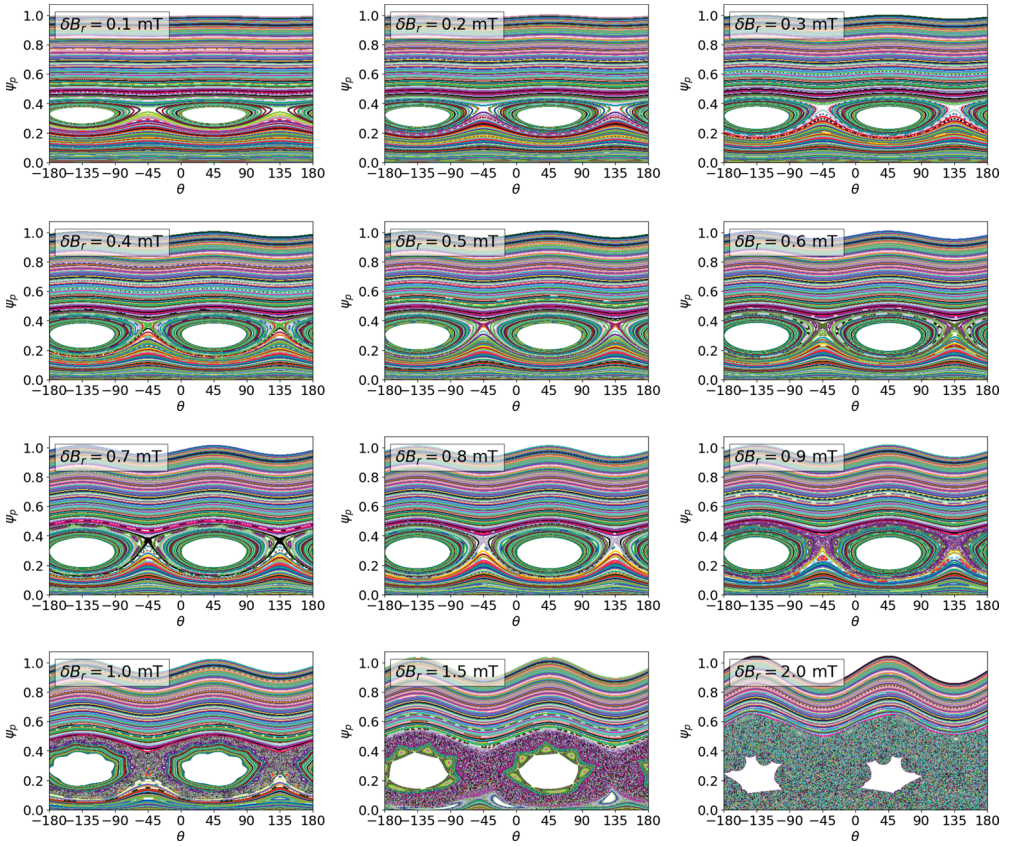

FIGURE 6. Poincaré sections of the plasma response as computed by M3D-C^1 and evaluated at $t = 5000\tau_A$ for 0.1 mT $\leq \delta B_r \leq$ 2 mT. Shown here as a function of normalised poloidal flux, ψ_p, and poloidal angle, θ.

perpendicular heat conductivity, where $\kappa_\parallel/\kappa_t \gg 1$. On the other hand, in the MRxMHD model there is assumed to be no perpendicular heat diffusion. As a consequence, pressure gradients cannot be supported across magnetic islands or in regions of magnetic field line chaos. It is to be expected that the SPEC and M3D-C^1 results will diverge when the effect of finite perpendicular heat conductivity becomes significant, although the differences may diminish for $\kappa_\parallel/\kappa_t$ significantly larger than the value considered in this work (Hudson 2009).

5.2. *Properties of the RMP response calculated with SPEC*

As in § 5.1, we start from the initial axisymmetric equilibrium given by (2.1) and (2.2) and, this time, use the procedure described in § 3 to calculate MRxMHD solutions to an $(m = 2, n = 1)$ perturbation of the plasma boundary, with amplitude Δr_a. Specifically, we consider 0.01 mm $\leq \Delta r_a <$ 20 mm which, using (4.20), corresponds to 0.0053 mT $\leq \delta B_r <$ 1 mT. As discussed in § 3, we considered a fixed number of volumes, $N_{\text{vol}} = 5$, which is representative of practical use cases for the code, including in the context of modelling experimental measurements.

A key parameter for SPEC calculations is the amount of normalised toroidal flux, $\Psi_{t,i}$, in each ith volume. This parameter has two important consequences. Firstly, the flux in

https://doi.org/10.1017/S0022377822000927 Published online by Cambridge University Press

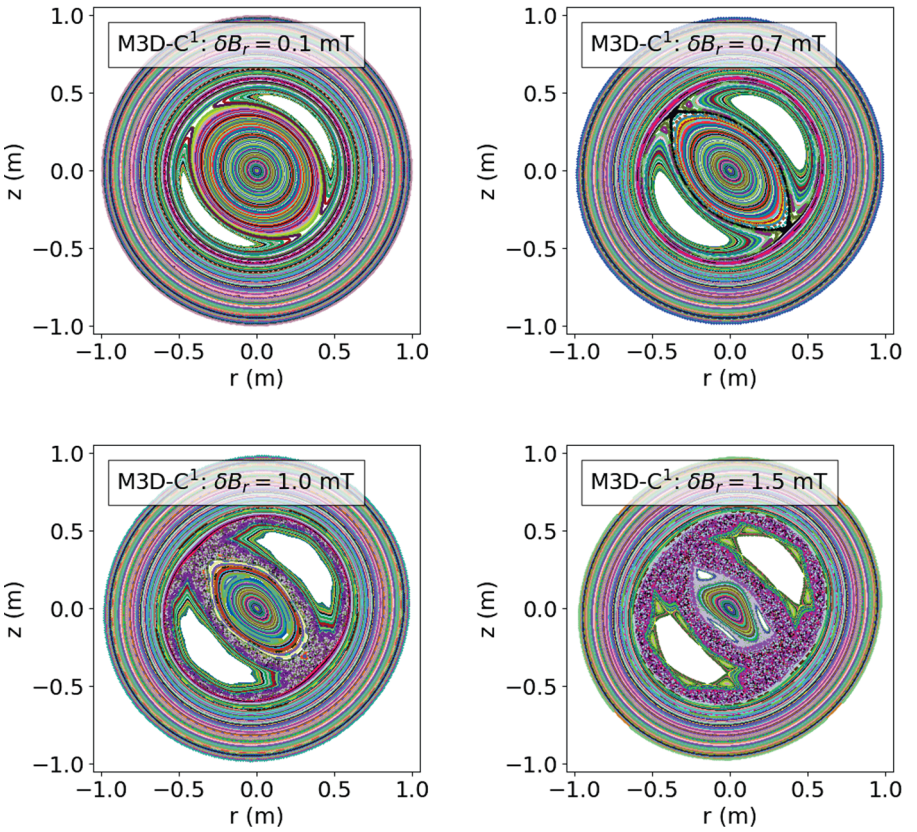

FIGURE 7. Poincaré sections of the plasma response as computed by M3D-C^1 and evaluated at $t = 5000\tau_A$ for $\delta B_r = 0.1,\ 0.7,\ 1,\ 1.5$ mT. The pressure profiles shown in figure 8 correspond to cuts taken along $z = 0$.

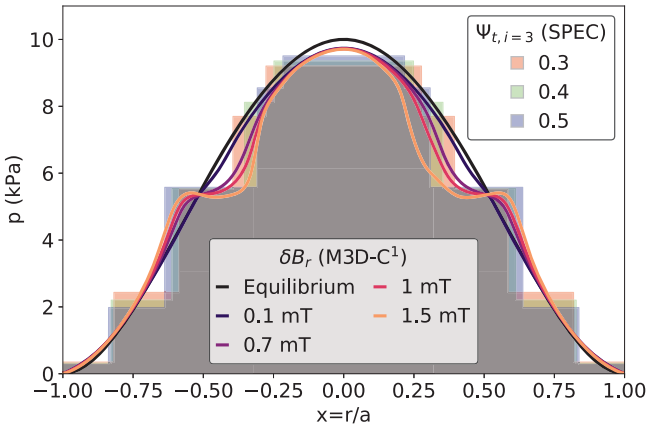

FIGURE 8. Pressure profiles at $t = 5000\tau_A$ as computed by M3D-C^1 shown as a cut taken along $z = 0$ for $\delta B_r = 0.1,\ 0.7,\ 1,\ 1.5$ mT (solid lines). Also shown is the equilibrium pressure profile (black line), given by (2.2). For comparison, the discretised pressure profiles used in the SPEC calculations are represented by filled curves for $\Psi_{t,i=3} = 0.3$ (red), 0.4 (green) and 0.5 (blue).

https://doi.org/10.1017/S0022377822000927 Published online by Cambridge University Press

each volume (which is held fixed during every SPEC solve) impacts the position of the interfaces in real space. This controls the spatial locations at which the original equilibrium profiles are discretised and, in turn, affects the fidelity of the discrete representation that is used by SPEC. This is particularly true for cases where N_{vol} is relatively small, as is considered presently.

As will be seen, the value of $\Psi_{t,i}$ in the volume containing the resonant surface of interest also has a strong effect on the properties of the magnetic islands that are computed by SPEC. In particular, the island width depends strongly on $\Psi_{t,i}$ in the volume of interest, which is consistent with what has been observed previously in SPEC calculations performed in a slab geometry (Loizu *et al.* 2015).

We also find that the relative position, with respect to $\Psi_{t,i}$, of the resonant surface of interest within the volume affects the shape of the resultant islands. Specifically, where the resonant surface is closer to one of the two bounding interfaces than the other (in terms of enclosed toroidal flux), the islands become distorted and deviate from the physically expected result. Therefore, for this study we took particular care to ensure that the $q = 2$ resonant surface (which lies in the third volume) was centred with respect to $\Psi_{t,i=3}$. This was achieved by carefully prescribing the value of $\iota = 1/q$ for each interface in the 'fixed iota' step of the calculation procedure (see figure 5) and amounts to a particular discretisation of the q-profile. While possible in this work, the procedure adopted here may not be universally applicable because, in the general 3-D setting, the MRxMHD model requires interfaces to be associated only with surfaces that have sufficiently irrational ι, in the sense of KAM theory. Since the existence of these KAM invariant tori is closely related to the shape of the surfaces (McGann *et al.* 2010), the discretisation of the q-profile in the most general case is effectively fixed by the geometry of the problem.

5.3. *Comparing the nonlinear RMP response in SPEC*

In figure 9 we compare the island widths obtained from M3D-C^1 and SPEC for $\Psi_{t,i=3} = 0.3, 0.4$ and 0.5. The shaded regions correspond to the error bars associated with measurement of the island widths, which are obtained from field line tracing and examination of the Poincaré sections. As seen in figure 6, for $\delta B_r \geq 0.6$ mT we begin to observe significant stochasticisation of the separatrix associated with the primary $(m = 2, n = 1)$ island chain in M3D-C^1. In these cases, the island 'widths' shown in figure 9 are calculated by considering the distance between the two nearest flux surfaces bounding the islands and/or chaotic volume. Clearly, for $\delta B_r = 2$ mT where we observe complete stochasticisation of the plasma core (figure 6, bottom right), no such quantity can be calculated.

As already alluded to, in figure 9 we find a strong dependence of the SPEC island widths on $\Psi_{t,i=3}$, the normalised toroidal flux in the volume containing the $q = 2$ rational surface. Increasing $\Psi_{t,i=3}$ in SPEC allows for larger islands as the strength of the RMP increases. This is to be expected since the maximum possible width of the island is only what can be allowed based on the toroidal flux initially enclosed in the volume. As can be seen for $\Psi_{t,i=3} = 0.3$ and 0.4, if $\Psi_{t,i}$ is too small the size of the resultant islands is artificially limited. For $\delta B_r \leq 0.5$ mT, we observe the best overall agreement across this range of δB_r when $\Psi_{t,i=3} = 0.5$. In figure 10 we present an example of one such case (with $\delta B_r \approx 0.2$mT) showing good agreement between the SPEC and M3D-C^1 calculations of the plasma response, which consists of a saturated $(m = 2, n = 1)$ magnetic island at the $q = 2$ resonant surface. For the SPEC calculation, $N_{\text{vol}} = 5$ and $\Psi_{t,i=3} = 0.5$, while the M3D-C^1 solution is evaluated at $t = 5000\tau_A$.

At very small RMP amplitudes, particularly below $\delta B_r \sim 0.05$ mT, there is insufficient information in this study to conclusively determine which value of $\Psi_{t,i=3}$ gives the best

https://doi.org/10.1017/S0022377822000927 Published online by Cambridge University Press

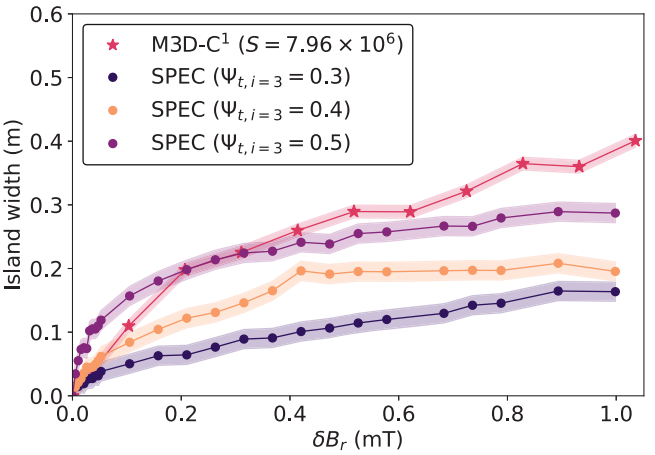

FIGURE 9. Saturated widths of ($m = 2, n = 1$) magnetic islands due to externally applied (2, 1) RMP fields, as calculated by M3D-C^1 (pink), and SPEC for $\Psi_{t,i=3} = 0.3$ (blue), $\Psi_{t,i=3} = 0.4$ (orange) and $\Psi_{t,i=3} = 0.5$ (purple), where $\Psi_{t,i=3}$ is the normalised toroidal flux enclosed in the volume containing the $q = 2$ surface.

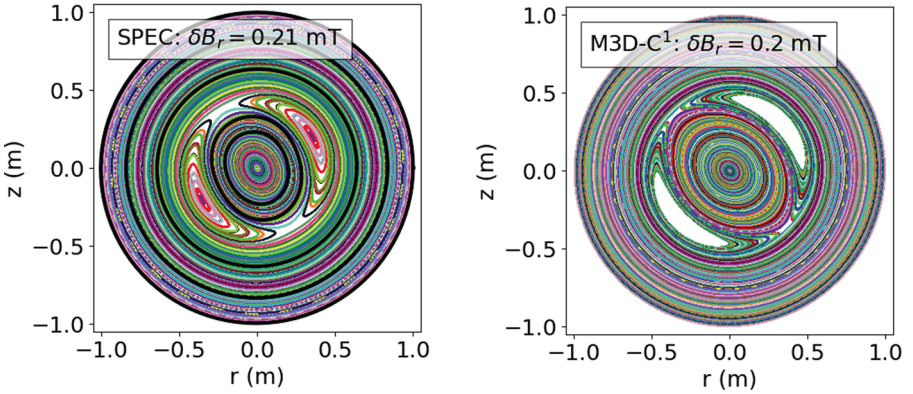

FIGURE 10. Poincaré sections of the plasma response as computed by SPEC (left, $\delta B_r = 0.21$ mT and $\Psi_{t,i=3} = 0.5$) and M3D-C^1 (right, $\delta B_r = 0.2$ mT). The SPEC interfaces are represented by black curves with $N_{\text{vol}} = 5$ and the M3D-C^1 solution is evaluated at $t = 5000\tau_A$.

agreement between SPEC and M3D-C^1. This underscores an overarching observation, which is the sensitivity of the island properties as calculated by SPEC to the value of $\Psi_{t,i=3}$. Because of the freedom that (to varying degrees) exists to prescribe $\Psi_{t,i}$, this effect is especially important when SPEC is used to calculate quantitative island properties, such as in recent applications of the code to stellarator optimisation (Landreman *et al.* 2021).

Particularly for $\Psi_{t,i=3} = 0.5$, we observe that the SPEC island widths, w, scale approximately as $\delta B_r^{1/2}$ for the values of δB_r considered. According to theory (Wesson & Campbell 2011), this implies that the resonant component of the total magnetic field at the $q = 2$ surface, δB, remains linearly proportional to δB_r, the driving field at the plasma edge.

There are two conditions under which we expect island width to scale differently to $\delta B_r^{1/2}$. The first is when the island size is no longer small compared with equilibrium scale lengths such as the minor radius. From figure 7, we see that significant islands can open

https://doi.org/10.1017/S0022377822000927 Published online by Cambridge University Press

up in the M3D-C^1 solution, even for $\delta B_r = 0.1$ mT. It is expected that the inclusion of equilibrium flows would lead to a significant reduction of the island size. While M3D-C^1 can accommodate states with equilibrium flows, work to extend the MRxMHD model to incorporate flows is ongoing. Consequently, we were limited to the static version of the MRxMHD model for this study and, therefore, do not consider the effect of equilibrium flows.

The island width scaling can also be modified when the resonant component of the field at the $q = 2$ surface is no longer linearly proportional to the driving field, i.e. no longer satisfying $\delta B \propto \delta B_r$. This is indicative of significant nonlinearity in the plasma response, such as shielding or amplification of the applied RMP field. At larger δB_r, figure 9 suggests that for $\Psi_{t,i=3} = 0.5$ the response computed by SPEC remains largely linear insomuch that $\delta B \propto \delta B_r$ since $w \propto \delta B_r^{1/2}$. In contrast, solutions calculated by the M3D-C^1 model, which has been extensively validated and used to model the plasma response (both linear and nonlinear) to externally applied 3-D fields in a range of applications (Ferraro *et al.* 2013; Reiman *et al.* 2015; Wingen *et al.* 2015; Canal *et al.* 2017; Lyons *et al.* 2017), shows a clear deviation from the square-root scaling at larger δB_r. This suggests that nonlinear mechanisms, leading to shielding and/or amplification of the applied RMP field, contribute significantly to the plasma response. While beyond the scope of the present work, further elucidating the physics properties of the plasma response predicted by the MRxMHD model would be valuable as part of future work. In particular, examining the resonant component of the magnetic field at the corresponding rational surface to identify linear and nonlinear contributions to the plasma response.

5.4. *Robustness and sensitivity of SPEC solutions*

SPEC uses Newton methods to solve for both the Beltrami fields (3.1) and the interface geometry (3.2) and, as a consequence, can become sensitive to small changes in parameters such as Δr_a. We observed this to be the case for larger perturbation amplitudes, where $\delta B_r > 0.5$ mT. An example of this is illustrated in figure 11. As in figure 10, $N_{\text{vol}} = 5$ and $\Psi_{t,i=3} = 0.5$ in the SPEC calculation, while the M3D-C^1 solution is evaluated at $t = 5000\tau_A$. For $\delta B_r = 0.7$ mT, the plasma response obtained from M3D-C^1 is characterised by a saturated ($m = 2, n = 1$) island at the $q = 2$ resonant surface and about which there is a higher m secondary island chain. In contrast, for $\delta B_r = 0.683$mT and $\delta B_r = 0.736$ mT, which differ only slightly, we observe two qualitatively different solutions for the plasma response as calculated by SPEC, both of which differ from the M3D-C^1 response. In particular, for $\delta B_r = 0.736$ mT we observe the appearance of a high m island chain in an inner volume which does not contain the $q = 2$ resonant surface.

As a measure of robustness, we consider the residual force error which represents the net force on each interface and, therefore, the difference between the numerical solution and the equilibrium condition, (3.2). For $\delta B_r \leq 0.5$ mT, at fixed Fourier resolution, the force error is $O(10^{-12})$ or less and, for $\Psi_{t,i=3} = 0.5$, we find good agreement between SPEC and M3D-C^1 (see figure 9). However, at the same Fourier resolution, for $\delta B_r \geq 0.6$ mT we find that the force error becomes very sensitive to small changes in Δr_a. In this regime, we observed that even when the force error was at most $O(10^{-13})$, a change of $\Delta r_a = 0.1$ mm could be sufficient to yield solutions with qualitatively different characteristics, e.g. a single ($m = 2, n = 1$) island chain vs. islands embedded in a chaotic sea.

One strategy for reducing sensitivity is to choose an initial guess that is close to the desired solution. This may be achieved, for example, by starting from an axisymmetric solution and constructing a sequence of solutions while incrementally increasing a parameter of interest (such as Δr_a) until the desired value is reached. Such an approach

https://doi.org/10.1017/S0022377822000927 Published online by Cambridge University Press

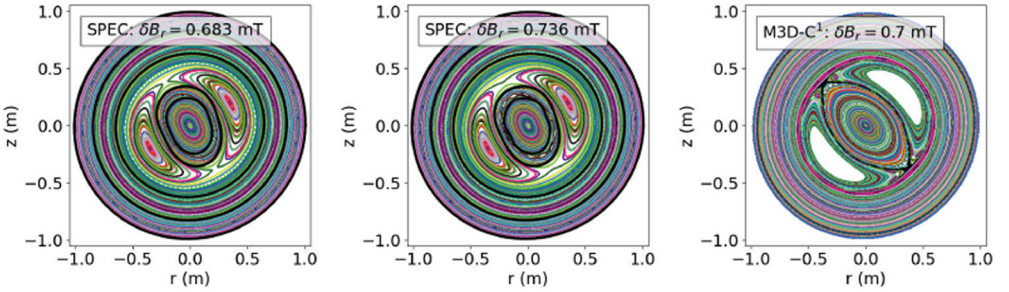

FIGURE 11. Poincaré sections of the plasma response as computed by SPEC (left, $\delta B_r = 0.683$ mT and $\Psi_{t,i=3} = 0.5$) and (centre, $\delta B_r = 0.736$ mT and $\Psi_{t,i=3} = 0.5$) and M3D-C^1 (right, $\delta B_r = 0.7$ mT). The SPEC interfaces are represented by black curves with $N_{\text{vol}} = 5$ and the M3D-C^1 solution is evaluated at $t = 5000\tau_A$.

requires the calculation of a large number of solutions, which is time consuming and, thus, not a universally viable strategy.

The observed decrease in robustness in the strongly driven RMP regime ($\delta B_r > 0.5$ mT) has important implications for applications including stellarator optimisation, where SPEC may be used to calculate quantitative properties of the equilibrium magnetic field structure. The ability to efficiently and reliably compute physics properties is essential for plasma optimisation procedures. In practice, parameters such as Fourier resolution are commonly specified in advance and held fixed during an optimisation run. On the other hand, Δr_a, which is related to the boundary shape, can change significantly in a free-boundary optimisation. We have seen, however, that the robustness of SPEC solutions can depend sensitively on both parameters.

6. Discussion and conclusions

In this work, we examined the conditions under which SPEC, an equilibrium code based on the MRxMHD model, can be used to model the nonlinear, non-ideal plasma response to externally applied symmetry-breaking magnetic field perturbations. In particular, we considered externally applied ($m = 2, n = 1$) RMP fields and compared solutions obtained from SPEC to a series of nonlinear simulations performed using the initial-value, extended-MHD code, M3D-C^1. Specifically, we consider perturbation amplitudes in the range $0.0053\ \text{mT} \leq \delta B_r \leq 1\ \text{mT}$.

First, we first developed a workflow for SPEC to compute the plasma response to a prescribed RMP, under conditions that represent experimentally relevant use cases. We described the discretisation of (smooth) equilibrium profiles, such as those which might be obtained from reconstruction of experimental measurements, and preparation of the input profiles required for SPEC.

We found that the normalised toroidal flux, $\Psi_{t,i}$, in the volume containing the resonant surface of interest is a key input parameter and has a significant effect on the properties of the magnetic islands that are computed by SPEC. For the work considered presently, the $q = 2$ surface is located in the $i = 3$ volume. We observed a strong dependence of the SPEC island width on $\Psi_{t,i=3}$. Importantly, when $\Psi_{t,i=3}$ was not large enough, we found that the maximum width of the islands, as calculated by SPEC, were artificially limited. Because there exists some freedom to choose $\Psi_{t,i}$ and since it must be prescribed *a priori* and remains fixed, this is particularly important when SPEC is used to calculate quantitative island properties, such as in some recent stellarator optimisation applications.

https://doi.org/10.1017/S0022377822000927 Published online by Cambridge University Press

Starting from an axisymmetric initial equilibrium, we used M3D-C^1 to simulate the nonlinear plasma evolution in response to $(m = 2, n = 1)$ RMP fields which were applied from $t = 0$. We considered RMP amplitudes in the range $0.1\ \text{mT} \leq \delta B_r \leq 2\ \text{mT}$ which, for an 0.1 T radial magnetic field at the plasma edge, corresponds to an RMP field strength of up to 2 %. For increasing RMP amplitudes, we observed four qualitatively distinct plasma responses in M3D-C^1; (i) a saturated $(m = 2, n = 1)$ magnetic island, (ii) formation of secondary island chains about the primary $(m = 2, n = 1)$ island, (iii) break up of the separatrix associated with the $(m = 2, n = 1)$ island and, eventually, (iv) complete stochasticisation of the plasma core.

Of the toroidal flux parameters considered in this study, we found that $\Psi_{t,i=3} = 0.5$ yielded the best overall agreement across the range of relatively small RMP amplitudes, where $\delta B_r \leq 0.5\ \text{mT}$. Above $\delta B_r > 0.5\ \text{mT}$, we observed a clear divergence between SPEC solutions and the nonlinear plasma response as determined by M3D-C^1. The critical RMP amplitude at which this occurred corresponds to the onset of secondary island chains and break up of the separatrix associated with the primary $(m = 2, n = 1)$ island. For this parameter range, in M3D-C^1 we observed significant pressure gradients in regions of chaotic magnetic fields. This is due to finite parallel heat conductivity that is not captured by SPEC. For $\delta B_r > 0.5\ \text{mT}$ we also encountered a marked decrease in the robustness of SPEC solutions, including finding that the qualitative features of SPEC solutions became highly sensitive to small changes in the amplitude of the applied RMP.

Given the strong dependence of the SPEC solution properties on the flux in the volume containing the resonant surface of interest, an obvious question that remains outstanding is how to determine this quantity *a priori*. To do so requires additional theoretical development and exploration of the underlying MRxMHD physics model, which is beyond the scope of the present work. However, this is a critical question to address if SPEC is to be used as predictive tool for modelling the plasma response to externally applied 3-D fields.

In this work, we focussed on the role of the toroidal flux in determining the physics properties of the SPEC solutions. The MRxMHD model justifies the existence of interfaces by requiring the corresponding q value to be 'sufficiently irrational', in the sense of KAM theory. Therefore, a related question is to understand the effect of the q-profile discretisation on the solutions as computed by SPEC. Preliminary studies suggest that this may introduce an additional source of sensitivity in SPEC, which motivates continued theoretical development of the MRxMHD model to better understand the connection between the underlying physics assumptions of MRxMHD and explicitly time-dependent extended-MHD models.

The ability to compute both the nonlinear and non-ideal plasma response to externally applied, symmetry-breaking magnetic field perturbations in realistic toroidal geometries is critical to a range of tokamak and stellarator applications. The ability to do so efficiently (in terms of both time and computational resources) opens up new opportunities in applications such as plasma optimisation and design. Our work indicates that SPEC is currently a viable tool for modelling the non-ideal plasma response to externally applied 3-D fields (including resonant magnetic perturbations and error fields) in the weakly nonlinear regime. Specifically, this means for perturbation amplitudes below the threshold for break up of the separatrix and onset of secondary magnetic island formation, and makes reliably identifying this critical value an important task for future work. Finally, future numerical improvements to SPEC, together with continued theoretical development of the MRxMHD model, may extend the parameter regime in which SPEC is a viable tool for modelling the plasma response to externally applied 3-D fields, by addressing outstanding questions, including how to prescribe $\Psi_{t,i}$ and N_{vol}.

https://doi.org/10.1017/S0022377822000927 Published online by Cambridge University Press

Acknowledgements

Editor William Dorland thanks the referees for their advice in evaluating this article.

Declaration of interest

The authors report no conflict of interest.

Funding

This work was supported by Department of Energy Contract No. DE-AC02-09-CH11466 and the Summer Undergraduate Laboratory Internship (SULI) program.

REFERENCES

ALEYNIKOVA, K., HUDSON, S.R., HELANDER, P., KUMAR, A., GEIGER, J., HIRSCH, M., LOIZU, J., NÜHRENBERG, C., RAHBARNIA, K. & QU, Z. 2021 Model for current drive induced crash cycles in W7-X. *Nucl. Fusion* **61** (12), 126040.

ARNOLD, V.I. 1963 Proof of a theorem of A.N. Kolmogorov on the preservation of conditionally periodic motions under a small perturbation of the Hamiltonian. *Russian Mathematical Surveys* **18** (5), 9.

BOOZER, A.H. & NÜHRENBERG, C. 2006 Perturbed plasma equilibria. *Phys. Plasmas* **13** (10), 102501.

CALLEN, J.D. 2011 Effects of 3D magnetic perturbations on toroidal plasmas. *Nucl. Fusion* **51** (9), 094026.

CANAL, G.P., FERRARO, N.M., EVANS, T.E., OSBORNE, T.H., MENARD, J.E., AHN, J.-W., MAINGI, R., WINGEN, A., CIRO, D., FRERICHS, H., SCHMITZ, O., SOUKHANOVISKII, V., WATERS, I. & SABBAGH, S.A. 2017 M3D-C1 simulations of the plasma response to RMPs in NSTX-U single-null and snowflake divertor configurations. *Nucl. Fusion* **57** (7), 076007.

DEWAR, R.L., YOSHIDA, Z., BHATTACHARJEE, A. & HUDSON, S.R. 2015 Variational formulation of relaxed and multi-region relaxed magnetohydrodynamics. *J. Plasma Phys*. **81** (6), 515810604.

EVANS, T.E., *et al.* 2004 Suppression of large edge-localized modes in high-confinement DIII-D plasmas with a stochastic magnetic boundary. *Phys. Rev. Lett*. **92**, 235003.

EVANS, T.E., *et al.* 2008 RMP ELM suppression in DIII-D plasmas with ITER similar shapes and collisionalities. *Nucl. Fusion* **48** (2), 024002.

EVANS, T.E., MOYER, R.A., BURRELL, K.H., FENSTERMACHER, M.E., JOSEPH, I., LEONARD, A.W., OSBORNE, T.H., PORTER, G.D., SCHAFFER, M.J., SNYDER, P.B., *et al.* 2006 Edge stability and transport control with resonant magnetic perturbations in collisionless tokamak plasmas. *Nat. Phys*. **2** (6), 419–423.

FERRARO, N.M. 2012 Calculations of two-fluid linear response to non-axisymmetric fields in tokamaks. *Phys. Plasmas* **19** (5), 056105.

FERRARO, N.M., EVANS, T.E., LAO, L.L., MOYER, R.A., NAZIKIAN, R., ORLOV, D.M., SHAFER, M.W., UNTERBERG, E.A., WADE, M.R. & WINGEN, A. 2013 Role of plasma response in displacements of the tokamak edge due to applied non-axisymmetric fields. *Nucl. Fusion* **53** (7), 073042.

FURTH, H.P., RUTHERFORD, P.H. & SELBERG, H. 1973 Tearing mode in the cylindrical tokamak. *Phys. Fluids* **16** (7), 1054–1063.

HAHM, T.S. & KULSRUD, R.M. 1985 Forced magnetic reconnection. *Phys. Fluids* **28** (8), 2412–2418.

HEGNA, C.C. 2014 Effects of a weakly 3-D equilibrium on ideal magnetohydrodynamic instabilities. *Phys. Plasmas* **21** (7), 072502.

HIRSHMAN, S.P., SANCHEZ, R. & COOK, C.R. 2011 SIESTA: A scalable iterative equilibrium solver for toroidal applications. *Phys. Plasmas* **18** (6), 062504. https://doi.org/10.1063/1.3597155

HIRSHMAN, S.P. & WHITSON, J.C. 1983 Steepest-descent moment method for three-dimensional magnetohydrodynamic equilibria. *Phys. Fluids* **26** (12), 3553–3568.

HOELZL, M., *et al.* 2021 The JOREK non-linear extended MHD code and applications to large-scale instabilities and their control in magnetically confined fusion plasmas. *Nucl. Fusion* **61** (6), 065001.

HOLE, M.J., HUDSON, S.R. & DEWAR, R.L. 2006 Stepped pressure profile equilibria in cylindrical plasmas via partial Taylor relaxation. *J. Plasma Phys*. **72** (6), 1167–1171.

HOLE, M.J., HUDSON, S.R. & DEWAR, R.L. 2007 Equilibria and stability in partially relaxed plasma–vacuum systems. *Nucl. Fusion* **47** (8), 746–753.

HOSKING, R.J. & DEWAR, R.L. 2016 *Fundamental Fluid Mechanics and Magnetohydrodynamics*. Springer.

HUANG, Y.-M., HUDSON, S.R., LOIZU, J., ZHOU, Y. & BHATTACHARJEE, A. 2021 Numerical approach to δ-function current sheets arising from resonant magnetic perturbations. arXiv:2108.09327.

HUDSON, S.R. 2009 An expression for the temperature gradient in chaotic fields. *Phys. Plasmas* **16** (1), 010701.

HUDSON, S.R., DEWAR, R.L., DENNIS, G., HOLE, M.J., MCGANN, M., VON NESSI, G. & LAZERSON, S. 2012 Computation of multi-region relaxed magnetohydrodynamic equilibria. *Phys. Plasmas* **19** (11), 112502.

IMBERT-GERARD, L.-M., PAUL, E.J. & WRIGHT, A.M. 2020 An introduction to stellarators: from magnetic fields to symmetries and optimization. arXiv:1908.05360.

IZZO, V.A. & JOSEPH, I. 2008 RMP enhanced transport and rotational screening in simulations of DIII-D plasmas. *Nucl. Fusion* **48** (11), 115004.

JARDIN, S.C., FERRARO, N., BRESLAU, J. & CHEN, J. 2012 Multiple timescale calculations of sawteeth and other global macroscopic dynamics of tokamak plasmas. *Comput. Sci. Disc*. **5** (1), 014002.

KOLMOGOROV, A.N. 1954 On the conservation of conditionally periodic motions under small perturbation of the Hamiltonian. In *Doklady Akademii Nauk SSSR*, vol. 98, pp. 2–3.

LANDREMAN, M., MEDASANI, B., WECHSUNG, F., GIULIANI, A., JORGE, R. & ZHU, C. 2021 SIMSOPT: A flexible framework for stellarator optimization. *J. Open Source Softw*. **6** (65), 3525.

LAO, L.L., JOHN, H.S.., STAMBAUGH, R.D., KELLMAN, A.G. & PFEIFFER, W. 1985 Reconstruction of current profile parameters and plasma shapes in tokamaks. *Nucl. Fusion* **25** (11), 1611–1622.

LIU, Y.Q., BONDESON, A., FRANSSON, C.M., LENNARTSON, B. & BREITHOLTZ, C. 2000 Feedback stabilization of nonaxisymmetric resistive wall modes in tokamaks. I. Electromagnetic model. *Phys. Plasmas* **7** (9), 3681–3690.

LOIZU, J., HUANG, Y.-M., HUDSON, S.R., BAILLOD, A., KUMAR, A. & QU, Z.S. 2020 Direct prediction of nonlinear tearing mode saturation using a variational principle. *Phys. Plasmas* **27** (7), 070701.

LOIZU, J., HUDSON, S., BHATTACHARJEE, A. & HELANDER, P. 2015 Magnetic islands and singular currents at rational surfaces in three-dimensional magnetohydrodynamic equilibria. *Phys. Plasmas* **22** (2), 022501.

LYONS, B.C., FERRARO, N.M., PAZ-SOLDAN, C., NAZIKIAN, R. & WINGEN, A. 2017 Effect of rotation zero-crossing on single-fluid plasma response to three-dimensional magnetic perturbations. *Plasma Phys. Control. Fusion* **59** (4), 044001.

MCGANN, M., HUDSON, S.R., DEWAR, R.L. & VON NESSI, G. 2010 Hamilton-Jacobi theory for continuation of magnetic field across a toroidal surface supporting a plasma pressure discontinuity. *Phys. Lett.* A **374** (33), 3308–3314.

MÖSER, J. 1962 On invariant curves of area-preserving mappings of an annulus. In *Nachrichten der Akademie der Wissenschaften in Göttingen II*, pp. 1–20. Vanderhoeck & Ruprecht.

NÜHRENBERG, C. & BOOZER, A.H. 2003 Magnetic islands and perturbed plasma equilibria. *Phys. Plasmas* **10** (7), 2840–2851.

ORAIN, F., BÉCOULET, M., MORALES, J., HUIJSMANS, G.T.A., DIF-PRADALIER, G., HOELZL, M., GARBET, X., PAMELA, S., NARDON, E., PASSERON, C., LATU, G., FIL, A. & CAHYNA, P. 2014 Non-linear MHD modeling of edge localized mode cycles and mitigation by resonant magnetic perturbations. *Plasma Phys. Control. Fusion* **57** (1), 014020.

PARK, J.-K., BOOZER, A.H. & GLASSER, A.H. 2007 Computation of three-dimensional tokamak and spherical torus equilibria. *Phys. Plasmas* **14** (5), 052110.

PARK, J.-K. & LOGAN, N.C. 2017 Self-consistent perturbed equilibrium with neoclassical toroidal torque in tokamaks. *Phys. Plasmas* **24** (3), 032505.

PARK, W., MONTICELLO, D.A., STRAUSS, H. & MANICKAM, J. 1986 Three-dimensional stellarator equilibrium as an ohmic steady state. *Phys. Fluids* **29** (4), 1171–1175.

PIRON, L., KIRK, A., LIU, Y.Q., CUNNINGHAM, G., CARR, M., GOWLAND, R., KATRAMADOS, I. & MARTIN, R. 2020 Error field correction strategies in preparation to MAST-U operation. *Fusion Engng Design* **161**, 111932.

REIMAN, A., FERRARO, N.M., TURNBULL, A., PARK, J.K., CERFON, A., EVANS, T.E., LANCTOT, M.J., LAZARUS, E.A., LIU, Y., MCFADDEN, G., MONTICELLO, D. & SUZUKI, Y. 2015 Tokamak plasma high field side response to an n= 3 magnetic perturbation: a comparison of 3D equilibrium solutions from seven different codes. *Nucl. Fusion* **55** (6), 063026.

REIMAN, A. & GREENSIDE, H. 1986 Calculation of three-dimensional MHD equilibria with islands and stochastic regions. *Comput. Phys. Commun*. **43**, 157.

SINGH, L., KRUGER, T.G., BADER, A., ZHU, C., HUDSON, S.R. & ANDERSON, D.T. 2020 Optimization of finite-build stellarator coils. *J. Plasma Phys*. **86** (4), 905860404.

SOVINEC, C.R., GIANAKON, T.A., HELD, E.D., KRUGER, S.E. & SCHNACK, D.D. 2003 NIMROD: A computational laboratory for studying nonlinear fusion magnetohydrodynamics. *Phys. Plasmas* **10** (5), 1727–1732.

SUZUKI, Y. 2017 HINT modeling of three-dimensional tokamaks with resonant magnetic perturbation. *Plasma Phys. Control. Fusion* **59** (5), 054008.

SUZUKI, Y., NAKAJIMA, N., WATANABE, K., NAKAMURA, Y. & HAYASHI, T. 2006 Development and application of HINT2 to helical system plasmas. *Nucl. Fusion* **46** (11), L19–L24.

TURNBULL, A.D. 2012 Plasma response models for non-axisymmetric perturbations. *Nucl. Fusion* **52** (5), 054016.

TURNBULL, A.D., FERRARO, N.M., IZZO, V.A., LAZARUS, E.A., PARK, J.-K., COOPER, W.A., HIRSHMAN, S.P., LAO, L.L., LANCTOT, M.J., LAZERSON, S., LIU, Y.Q., REIMAN, A. & TURCO, F. 2013 Comparisons of linear and nonlinear plasma response models for non-axisymmetric perturbations. *Phys. Plasmas* **20** (5), 056114.

WESSON, J. & CAMPBELL, D.J. 2011 *Tokamaks*, vol. 149. Oxford University Press.

WINGEN, A., FERRARO, N.M., SHAFER, M.W., UNTERBERG, E.A., CANIK, J.M., EVANS, T.E., HILLIS, D.L., HIRSHMAN, S.P., SEAL, S.K., SNYDER, P.B. & SONTAG, A.C. 2015 Connection between plasma response and resonant magnetic perturbation (RMP) edge localized mode (ELM) suppression in DIII-D. *Plasma Phys. Control. Fusion* **57** (10), 104006.

ZHOU, Y., FERRARO, N.M., JARDIN, S.C. & STRAUSS, H.R. 2021 Approach to nonlinear magnetohydrodynamic simulations in stellarator geometry. *Nucl. Fusion* **61** (8), 086015.

ZHU, C., GATES, D.A., HUDSON, S.R., LIU, H., XU, Y., SHIMIZU, A. & OKAMURA, S. 2019 Identification of important error fields in stellarators using the hessian matrix method. *Nucl. Fusion* **59** (12), 126007.

ZHU, C., HUDSON, S.R., LAZERSON, S.A., SONG, Y. & WAN, Y. 2018 Hessian matrix approach for determining error field sensitivity to coil deviations. *Plasma Phys. Control. Fusion* **60** (5), 054016.